International Journal of Multiphase Flow 115 (2019) 126–136

Contents lists available at ScienceDirect

International Journal of Multiphase Flow

journal homepage: www.elsevier.com/locate/ijmulflow

Degassing of a decompressed flowing liquid under hypergravity conditions

Ourania Oikonomidou[a], Sotiris P. Evgenidis[a], Christian J. Schwarz[b], Jack J.W.A. van Loon[b,c], Margaritis Kostoglou[a], Thodoris D. Karapantsios[a,*]

[a] Division of Chemical Technology, School of Chemistry, Aristotle University of Thessaloniki, University Box 116, 541 24 Thessaloniki, Greece
[b] Life Support and Physical Sciences Section, European Space Agency - European Space Research and Technology Centre (ESA-ESTEC), Keplerlaan 1, 2200 AG, Noordwijk, the Netherlands
[c] DESC (Dutch Experiment Support Center), Amsterdam UMC and Academic Centre for Dentistry Amsterdam (ACTA), Vrije Universiteit Amsterdam, Department of Oral and Maxillofacial Surgery/Pathology, Amsterdam Movement Sciences, de Boelelaan 1117, Amsterdam, the Netherlands

ARTICLE INFO

Article history:
Received 27 August 2018
Revised 15 February 2019
Accepted 31 March 2019
Available online 1 April 2019

Keywords:
Degassing
Hypergravity
Buoyancy
Centrifuge
bubble velocity
Decompression

ABSTRACT

The formation and growth of bubbles due to decompression degassing of a liquid has been extensively studied in the past, aiming to enhance the efficiency of specific industrial applications. Even though liquid decompression degassing may interfere with the performance of space processes (such as cooling and lubrication systems, combustion and storage of liquid propellants etc.), the phenomenon has never been studied in non-terrestrial gravity conditions. The present work investigates for the first time, bubbles dynamics of a degassing liquid under various hypergravity accelerations. Degassing bubbles form due to desorption of dissolved air upon decompression of a liquid jet partially saturated with air. Accelerations up to 12 g are applied artificially by means of the Large Diameter Centrifuge facility of the European Space Agency. A patented electrical impedance spectroscopy technique provides the distribution of desorbed gas along the flow. Analysis of high resolution images indicates changes of bubbles size. Residence time distributions using conductivity tracers reveal the flow pattern in the degassing vessel. The total extent of liquid degassing is derived from dissolved oxygen measurements. Hypergravity alters the bubbles velocity and, consequently, their residence time in the liquid. Therefore, it affects the gas fraction in the degassing vessel offering unique conditions for studying the impact of acceleration on bubble dynamics. Experimental findings are useful not only for the optimization of space processes during hypergravity phases, e.g., space vehicles launch and re-orbiting, but also for the construction of controlled degassing industrial applications.

1. Introduction

Degassing of a liquid constitutes a common industrial and biological process that, either spontaneously or deliberately, leads to formation of a gas-liquid two-phase medium. Bubbles generated during liquid degassing are customary characterized by their small size and narrow size distribution. These properties render degassing generated bubbles appropriate for a number of processes where good gas phase dispersity is required (Burns et al., 1997). Dissolved Air Flotation (DAF) process uses degassing bubbles to thicken activated sludge, to remove low density particles from potable water and to remove oil contaminants from wastewater (Radzuan et al., 2016). In other fields of application, degassing bubbles constitute the agent for the characteristic sparkling flavor of carbonated beverages (Liger-Belair et al., 2015) and for improving spray atomization in fine droplets (Caputo et al., 2010). However, in some applications it is vital to avoid degassing as it deteriorates either the materials quality or the process efficiency. Pumps pitting, wine oxidation, irregularities in glass or plastic molds and coatings, bacteria growth in crude oil and the advent of decompression sickness in divers and astronauts are some indicative detrimental effects of degassing (Chen, 1993; Lopes et al., 2009; Alshahrani et al., 2015; Birdi and Kleinitz1998; Papadopoulou et al., 2013). In some of the latter applications, partial liquid degassing is sometimes performed as a primary processing stage, aiming to free the working liquid from dissolved gases and thus prevent uncontrolled degassing later during the main process.

* Corresponding author.
E-mail addresses: oikonomid@chem.auth.gr (O. Oikonomidou), sevgenid@chem.auth.gr (S.P. Evgenidis), Fchristian.schwarz@esa.int (C.J. Schwarz), j.vanloon@vumc.nl (J.J.W.A. van Loon), kostoglu@chem.auth.gr (M. Kostoglou), karapant@chem.auth.gr (T.D. Karapantsios).

https://doi.org/10.1016/j.ijmultiphaseflow.2019.03.029
0301-9322/

The last decades, degassing of liquids has become a matter of great concern in aerospace applications as well. Alike to increasing the dispersion of a common spray, bubbles formation improves spreading of liquid propellants injected to the combustion chamber of a rocket (Huang et al., 1994). Liquid storage in space requires tanks resistant to oxidation in case of contact with desorbed oxygen (DeSain et al., 2015; Hearn and Coyle, 2007). Bubbles presence in coolants and lubricants inhibits thermal regulation of electronics and turbines in workstations and satellites (Chen et al., 2001; Sathyan et al., 2010). Admittedly, the behavior of bubbles in space has been reported mostly for microgravity conditions (Straub, 2005). Yet, science in space does not consider only phenomena occurring in the absence of gravity. During the launch or re-orbiting of space vehicles, rocket engines and boosters impose hypergravity accelerations to overcome the gravity of Earth or adjust vehicles' orbit. To our knowledge, the effect of hypergravity conditions on bubble dynamics has been reported only for boiling and gas sparging experiments (Lioumbas and Karapantsios, 2014; Sunol and Gonzalez-Cinca, 2015). Even though severe degassing may occur in space applications involving liquids, the dynamics of degassing bubbles have never been examined at increased gravitational accelerations.

For degassing to occur, a liquid supersaturated with dissolved gas is required. For instance, when a pressurized liquid containing dissolved gas is forced through a nozzle it experiences a substantial pressure drop. Consequently, the concentration of dissolved gas in the exiting liquid may largely exceed the equilibrium gas solubility associated with the nozzle exit pressure. As a result, bubble nuclei form in the liquid stream and a dissolved gas concentration gradient develops around the generated bubbles. Therefore, gas molecules diffuse from the liquid to the bubbles increasing their size (Soto et al., 2017). As bubbles grow, their boundaries expand and create additional flow as they push the surrounding liquid in the radial direction. The ensuing convection contributes to the overall bubbles size evolution (Mori, 1998). A second source of convective mass transfer is attributed to the relative bubble-liquid motion. Buoyancy is superimposed to the liquid flow and causes bubbles to rise faster than the liquid (Talaia, 2007). Bubbles interactions with their neighboring bubbles may cause additional changes to their size (Ponasse et al., 1998).

To harness the performance of liquid degassing, it is necessary to understand which parameters affect bubble dynamics and in what way. Many researchers have focused on determining the final size of degassing bubbles under the effect of several parameters, in an effort to define the optimum working conditions for Dissolved Air Flotation process. Dissolution pressure, nozzle geometry, liquid flow rate and liquid physical properties have been the most popular examined parameters (Takahashi et al., 1979; De Rijk et al., 1994; Ponasse et al., 1998). Their impact on bubble dynamics is different and sometimes debatable, as they may change simultaneously the level of supersaturation, the generated flow field and the force field applied to bubbles.

Recently, the controversial effect of dissolution pressure on the growth of degassing bubbles has been discussed (Oikonomidou et al., 2018). That work showed that the final size of bubbles is not exclusively determined by gas desorption, but it depends strongly on the complexity of the developing liquid flow field. In the intense mixing region above the exit of the nozzle, bubbles residence time increases and bubble size distributions get broader. The situation changes at some distance from the nozzle where plug flow prevails. In that region large bubbles merge with small ones due to gravitational coalescence and alter the overall size distributions. To shed light in the underlying phenomena, it is therefore necessary to simplify the flow field and isolate bubbles growth by gravitational coalescence from bubbles growth by gas desorption. The above is achieved in the present work, by employing a much shorter degassing device which limits development of the plug flow region. Going a step further, this study also aims to investigate the dynamics of degassing bubbles under varying relative bubble velocities. It is known that acceleration can act as a tool to alter bubbles rise velocity by modulating the buoyancy force (Kulkarni, 2005). The role of acceleration, however, is far more intriguing since it can affect bubbles size as well. Rapid bubble ascension provokes liquid flow, favors bubble collisions and limits the interfacial mass transport since the gas-liquid contact time becomes restricted.

The present work constitutes an attempt to validate by experimental evidence the crucial role of acceleration on bubbles dynamics during liquid degassing and on flow pattern development in a two-phase medium. Experiments are conducted at a variety of hypergravity acceleration values. The Large Diameter Centrifuge (LDC) facility of the European Space Agency (ESA/ESTEC) is used to create hypergravity conditions artificially (van Loon et al., 2008). Bubbles formation is triggered by applying different levels of supersaturation. The resulting two-phase flow is characterized regarding several aspects. Jet residence time distributions indicate possible changes of the flow pattern under different experimental conditions. Instantaneous volumetric gas fraction measurements at two locations inside the degassing vessel describe the dispersion of the desorbing gas phase along the flow. Optical observations yield the size distribution of the generated bubbles. Finally, the extent of liquid degassing is quantitatively estimated. Experimental results are extensively discussed regarding the contribution of acceleration on the characteristics of degassing bubbles.

2. Materials and methods

Fig. 1 presents the liquid degassing experimental apparatus constructed in compliance with the spatial constraints as well as the operational and safety regulations of the LDC. Fig. 2 is a schematic description of the employed experimental configuration. The studied liquid-gas system is water (with a conductivity

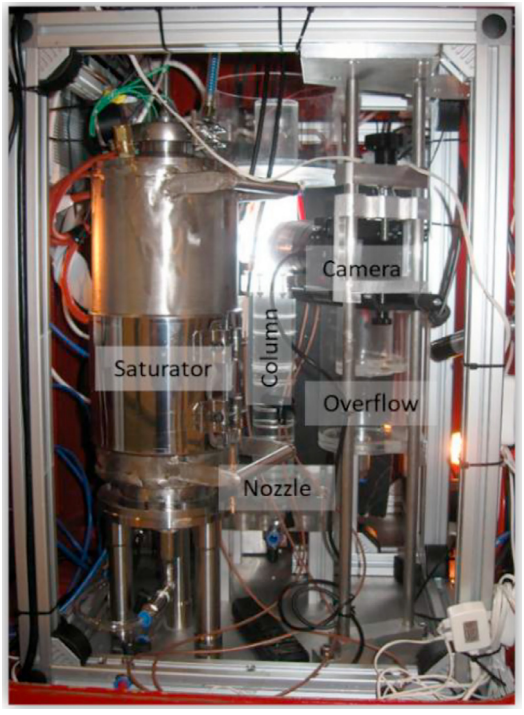

Fig. 1. Main parts of the liquid degassing experimental apparatus inside the centrifuge gondola.

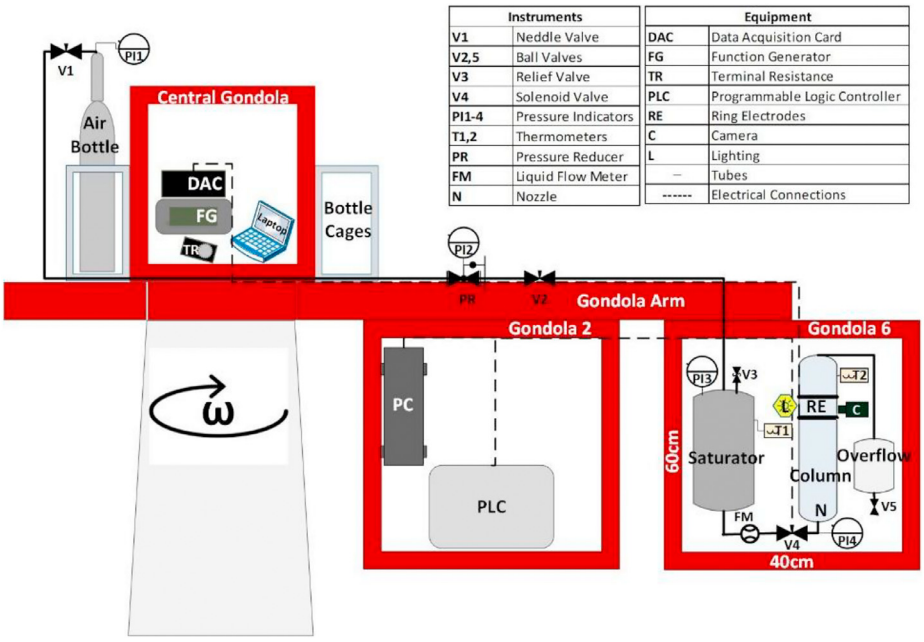

Fig. 2. Overview of experimental configuration within the LDC.

of 500 μS/cm) and atmospheric air at ambient temperature. Air is forced to dissolve in water at three different pressures 200 kPa, 300 kPa and 400 kPa (absolute pressures) inside a temperature controlled vessel called "saturator". The saturator contains 1.5 L of liquid and is connected to a compressed air bottle furnished with a pressure reducer. Air dissolution in water is achieved by vigorous shaking of the saturator for one minute. Intense convection currents and large liquid-gas interfacial area due to liquid sloshing amplify mass exchange. One minute of shaking proved enough for the pressure in the saturator to climb after an initial drop and remain thereafter constant at the prescribed gas dissolution pressure. The degree of air dissolution is measured by an optical Dissolved Oxygen probe (Pro ODO, YSI). Despite the employed vigorous shaking/sloshing, it has never been possible to reach full saturation of the liquid by dissolved gas. In fact, the achieved saturation has been always partial: 91% at 200 kPa, 86% at 300 kPa and 85% at 400 kPa. Such partial saturation levels are among the highest reported in the pertinent literature and are considered realistic in degassing investigations (Edzwald, 2007; Vlyssides et al., 2004; de Rijk and den Blanken, 1994; Hosokawa et al., 2009; Shannon, 1980). In view of brevity, however, the liquid in the saturator will henceforth be simply called saturated.

The degassing vessel is a transparent Plexiglas column connected to the saturator through flexible polyamide tubes. The column is 44 cm high with a diameter (D) of 4 cm and it is open to atmosphere. The column is initially filled to the top with water (0.55 L). A stainless-steel nozzle (N) 600 μm in diameter is located at the bottom center of the column. By opening the solenoid valve (V4) between the saturator and the degassing column, the saturated pressurized liquid passes through the nozzle and injects into the column. The liquid flow rate during injection is measured by a turbine flow meter (FHK-Ryton-10) (FM). The liquid jet exiting the nozzle gets supersaturated with dissolved gas because of the lower pressure in the column. Therefore, gas desorbs out of the liquid forming bubbles which grow due to mass diffusion and convection mechanisms. The experimental process resembles that of large scale liquid degassing experiments at terrestrial gravity reported by Oikonomidou et al. (2018).

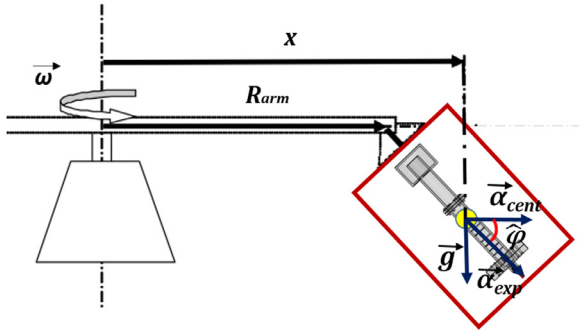

Fig. 3. Analysis of the artificial experimental acceleration ($\vec{\alpha}_{exp}$) developed during spinning of the LDC.

All hypergravity experiments are performed using the Large Diameter Centrifuge (LDC) facility at ESA/ESTEC Noordwijk, the Netherlands, along with experiments at terrestrial unit gravity to act as reference. The experimental setup is placed in one of the gondolas freely hanging from the LDC arms, Fig. 2. Hypergravity environment is accomplished artificially during the spinning of the LDC. Experimental acceleration ($\vec{\alpha}_{exp}$) results from the combination of centrifugal ($\vec{\alpha}_{cent}$) and gravitational ($\vec{g}$) accelerations as presented in Fig. 3. Since the gondola's radial distance from the center of rotation (R_{arm}) is fixed, variation of acceleration can be accomplished by changing the speed of rotation ($\vec{\omega}$). The free hanging gondola changes spontaneously its inclination ($\hat{\varphi}$) according to the employed speed of rotation to an extent that cancels the tangential acceleration component leaving only the normal component of acceleration applying to the gondola. As the gondola inclines, the degassing column inside the gondola acts as an extension of the LDC arm (x) along which the normal acceleration component increases with "x". More information regarding the forces applied during spinning of centrifuges are provided by Beysens and van Loon (2015) and van Loon et al. (2003).

Liquid degassing experiments are carried out under 2 g, 4 g, 8 g and 12 g normal acceleration components. These values refer

Table 1
Experimental conditions under the examined dissolution pressures and hypergravity accelerations.

	200kPa	300kPa	400kPa	
Q(L/min)	0.219	0.296	0.373	
Re_{jet}	7749	10473	13022	
U_{jet}(m/s)	12.9	17.3	22	
U_{flow}(mm/s)	2.9	3.9	4.9	
	2g	4g	8g	12g
ΔP compensation	+5kPa	+15kPa	+30kPa	+50kPa

exactly to the nozzle exit location. The desired acceleration level remains constant during each experimental run. The corresponding LDC angular velocity reaches steady state and only then liquid injection starts. Hypergravity makes the liquid hydrostatic pressure in the column to increase proportionally with the applied acceleration. Therefore, as hypergravity increases the pressure drop between the saturator and the exit of the nozzle is lower and this reduces the liquid flow rate. To maintain the same flow rate for each prescribed dissolution pressure, for all values of hypergravity, a small increase in the pressure inside the saturator is required in order to compensate for the hydrostatic pressure. To do so, upon completion of the gas dissolution process and just before liquid injection into the degassing vessel, the pressure in the saturator (PI3) is corrected by the corresponding additional hydrostatic pressure. In the absence of shaking/sloshing and because of the very short time interval until injection, this correction does not affect the extent of gas dissolution. Table 1 presents experimental parameters under different dissolution pressures and acceleration forces. Jet velocity at the nozzle exit (U_{jet}) equals the liquid flow rate (Q) divided by the nozzle cross-sectional area and flow velocity (U_{flow}) equals the liquid flow rate divided by the column cross-sectional surface. The last row of Table 1 shows the pressure correction applied to the saturator at every hypergravity level to compensate for the additional hydrostatic pressure in the column.

According to Stokes equation, the buoyancy velocity of bubbles increases with the acceleration. Consequently, the two-phase flow field developing during injection and degassing is quite complex. High jet velocities make the flow turbulent and chaotic, this being more so because of the progressive emergence of bubbles. So, to discriminate the phenomena imposed by the presence of bubbles, it is important to first characterize the flow field in the absence of bubbles. For this, a patented ultra-sensitive electrical impedance spectroscopy technique (Karapantsios et al., 2016) is utilized to study the residence time distribution of the water jet inside the column. The technique identifies the excitation current frequency with the highest ohmic response of the system, where capacitive and inductive electrical components are suppressed, and acquires data in envelopes circumscribed at 200 kHz which evades the parasitic influence of the mains and other stray currents. An extensive description of the technique is provided by Evgenidis and Karapantsios (2015). Liquids of different electrical conductivities are used to study the jet propagation at different dissolution pressures. During these "flow study" experiments, a high conductivity pressurized liquid (480 μS/cm) is injected into a low conductivity liquid preexisting in the column (240 μS/cm). The evolution of liquid electrical conductivity is recorded at 30 cm above the nozzle exit ($z/D = 7.5$, where "z" is the height along the column), during the whole injection period.

The same electrical impedance technique is also used to study gas phase formation during degassing of the supersaturated liquid injected at hypergravity conditions. During the injection period, the electrical resistance of the flow is continuously recorded at $z/D = 7.5$ above the nozzle exit. The recorded electrical data are transformed into volumetric gas fraction time series based on Maxwell's model.

The size distribution of degassing bubbles under various accelerations is studied optically using a SONY a6300 high resolution (24MP) still digital camera. Adequate magnification is accomplished combining a SONY E 30 mm f/3.5 Macro Lens with 52 mm long KENKO extension tubes. The camera is placed at $z/D = 7.5$ above the nozzle exit and focuses 3 mm ±0.5 mm away from the column walls ($r/R = 0.85$, where "r" is the radial distance from the column center and "R" is the column radius). Bubble images are captured automatically every 2 s during injection. A custom software computes the size distribution of bubbles in the captured images (Zabulis et al., 2007). For the shake of statistic accuracy, each bubble size distribution is estimated from 500 to 1500 sharp focused bubbles, contained in a series of consecutive images. The pixel/μm ratio is 1/1.93. The size per pixel calibration is accomplished using a string of specific thickness (56μm) as a reference scale. The different Indexes of Refraction (IR) of the mediums intervening the camera and the bubbles (air, plexiglass and water), combined to the curved column walls, distort the actual bubbles shape. Viewing at right angle the column, minimizes this effect. Yet, a mesh of standard geometry (immersed into the column) is used as a reference object to test the image distortion. It is found that the mesh vertical dimension is not affected by the presence of the various intervening interphases, so the size of bubbles is calculated based on bubbles vertical diameter during image processing.

Proper assessment of experimental findings requires evaluation of the total extent of degassing. This information is derived from the concentration of oxygen remaining dissolved in the liquid exiting the column. During injection, the liquid overflowing the column enters a 40 mL measuring tube. A dissolved oxygen optical probe is immersed in this tube, measuring instantaneously the dissolved oxygen concentration. Liquid supersaturation at the column exit indicates whether the total extent of liquid degassing varies with the applied acceleration.

3. Results

3.1. Flow pattern

The flow pattern in the degassing column, as illustrated by the residence time distribution, is presented in Fig. 4a. Bubbles presence is not desired in these "flow study" experiments, as they impose extra mixing to the flow (Oikonomidou et al., 2018). To avoid bubble formation in the degassing column, the liquid in the saturator is pressurized just before injection without applying any shaking/sloshing in order to suppress gas dissolution into the liquid. Experiments are conducted under terrestrial gravity conditions; however they are valid for every applied acceleration value since the effect of acceleration on liquid's hydrostatic pressure has been taken into account (as explained in the previous section). The curves in Fig. 4a correspond to different dissolution pressures in the saturator and therefore yield different decompression levels (ΔP) upon injection to the degassing column. The duration of

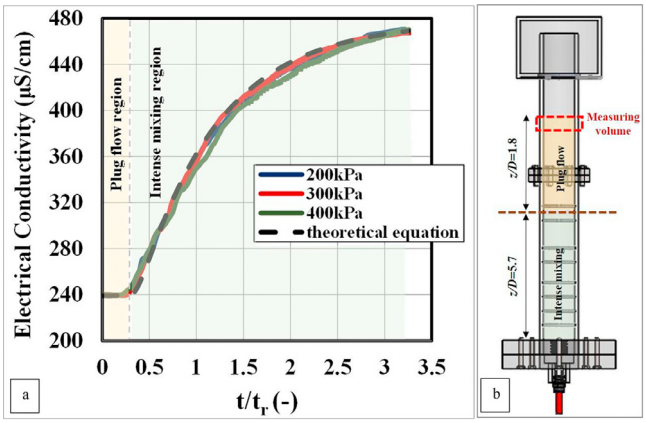

Fig. 4. (a) Jet residence time distributions using conductivity tracers at different dissolution pressures fitted by a theoretical equation, (b) distribution of the mixing and plug flow patterns along the column. Measuring volume refers to the location of electrical and optical measurements.

injection decreases with the applied dissolution pressure because the jet velocity increases proportionally to $\sqrt{\Delta P}$ while the total liquid volume in the saturator is always the same. Therefore, time (t) data series are normalized by the corresponding average residence time inside the column (t_r) to make the curves comparable (the average residence time equals the volume of the column up to $z/D = 7.5$, over the liquid flow rate). The resemblance among curves in Fig. 4a indicates that the flow behavior is not affected by the applied dissolution pressure. The increase of electrical conductivity with time denotes that the liquid bulk preexisting in the column is replaced gradually by the more conductive liquid entering during injection. At the first period of injection, $t/tr < 0.26$, the recorded electrical conductivity is constant which means that the liquid at $z/D = 7.5$ consists exclusively of the preexisting liquid. This implies that plug flow dominates at the top of the column. Once the injected (more conductive) liquid reaches the measuring location, electrical conductivity starts increasing and progressively approaches that of the injected liquid. The transition from initial to final conductivity is gradual, meaning that the jet creates a mixing region at the bottom part of the column. In order to quantify the above behavior and get a simplified prototype of the flow in the column, a 1-dimensional dispersion relation has been developed Eq. (1) for the residence time distribution.

$$\frac{\partial C}{\partial t} + U_{flow}\frac{\partial C}{\partial z} = \frac{\partial}{\partial z}E(z)\cdot\frac{\partial C}{\partial z} \tag{1}$$

where, C is the tracer concentration, assumed to have a linear relationship with the measured electrical conductivity.

z is the height along the column.
$E(z)$ is the dispersion coefficient as function of the height (z) along the column.

The above equation must be solved for the boundary conditions of the vertical distance along the column. Therefore:

$$U_{flow}\cdot(C - C_0) = E\cdot\frac{dC}{dz}, \text{at } z = 0 \quad \text{and} \quad \frac{dC}{dz} = 0, \text{at } z = Z$$

where $C_{(z,0)} = 0$ is the tracer concentration at time zero i.e. initial condition for Eq. (1).

C_0 is the tracer concentration at the inlet of the column ($z = 0$).
Z is the column height at the measuring location ($z/D = 7.5$).

The variable $C(Z, t)$ gives the residence time distribution for an assumed form of $E(z)$. Eq. (1) must be solved numerically since an analytical solution exists only for constant $E(z)$, even though it is complex and suffers convergence problems (Nauman and Buffham, 1983). The numerical solution is based on (a) discretization with second-order finite differences in the spatial domain and (b) an ordinary differential equation solver with self-adjustable step in the time domain. A searching procedure among different values of $E(z)$ that fulfills the above observations indicates that the functions $E = 0$ for $z > 22.8$ cm ($z/D = 5.7$) and $E = U_{flow}\cdot Z$ for $z < 22.8$ cm describe perfectly the experimental residence time distribution curves (see Fig. 4). Based on the above, the flow field inside the column consists of an intensively mixed region (although not fully mixed, as this would correspond to a much higher E) close to the jet, and a region of plug flow far above the jet.

3.2. Volumetric desorbed gas fractions

Fig. 5 shows the time evolution of the local volumetric desorbed gas fraction (ε), at $z/D = 7.5$ above the nozzle exit, under several hyper-gravity accelerations and dissolution pressures. At time zero there is already a fraction of gas at the measurement location of the column. However, this gas volume is not attributed to liquid degassing. It is gas trapped and compressed inside the tubing system of the device which escapes instantaneously from the nozzle at the moment of discharge and creates gas slugs into the column during the first seconds of injection. Such slugs travel rapidly towards the free surface of the liquid and do not influence the formation of degassing bubbles. When later during injection degassing bubbles reach the measuring volume, the slope of the curves turns positive. The more the column is filled with injected supersaturated liquid, the more the gas fraction increases. Oikonomidou et al. (2018), analyzing solely terrestrial gravity experiments, has shown that gas fractions close to the mixing region ($z/D = 7.5$) have twice the value of those measured at a larger

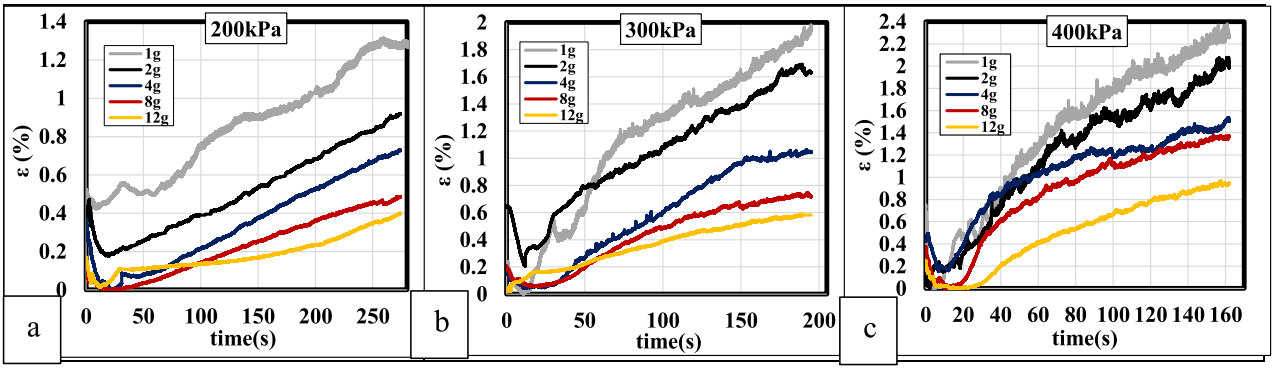

Fig. 5. The evolution of volumetric desorbed gas fraction (ε(%)) during the injection under different hypergravity accelerations and dissolution pressures (a) 200 kPa, (b) 300 kPa and (c) 400 kPa. Measurements are taken at $z/D = 7.5$.

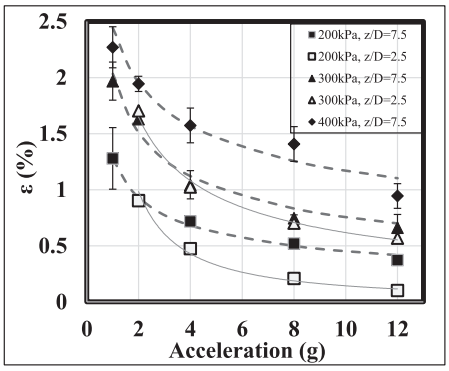

Fig. 6. Volumetric desorbed gas fraction ($\varepsilon(\%)$) at the end of the injection period, under different accelerations, dissolution pressures and locations within the column.

column height ($z/D = 22.5$). This was ascribed to bubbles being trapped and accumulated at a liquid recirculation loop in the mixing region.

It is interesting that for all the examined conditions in Fig. 5 the volumetric gas fraction never exceeds ~2.5%. Thus, bubbles can be assumed to flow as individual entities with only weak interaction with their neighbors. The positive slope of all curves suggests that gas fraction increases steadily in the column without ever managing to reach a plateau because of the relatively short period of the experiment (period of injection). This implies that in all runs there is remaining dissolved gas in the liquid at the end of injection. The amount of this remaining dissolved gas indicates whether the extent of degassing is governed exclusively by the applied extent of decompression or there is an effect of the applied acceleration, too (see below).

Fig. 6 presents the effect of hypergravity acceleration on the final volumetric desorbed gas fraction, measured at two column heights, $z/D = 7.5$ and $z/D = 2.5$, under different dissolution pressures. The presented experimental data refer to the end of the injection period, thus correspond to the same injected liquid volume to the column. Error bars result from three different repetitions under each experimental condition. Fig. 6 shows that the final concentration of desorbed gas fraction decreases with acceleration. To explain this behavior, the effect of acceleration on the mechanism of mass transfer between bubbles and liquid must be examined. Acceleration increases bubbles buoyancy velocity (U_b) and therefore minimizes bubbles residence time in the column. The restricted bubble/liquid contact time deteriorates the extent of mass transfer during liquid degassing, resulting in lower gas fractions. Moreover, acceleration broadens the difference between the velocities of large and small sized bubbles (ΔU_b) according to: $\Delta U_b \approx \alpha_{exp} \cdot (d_1^2 - d_2^2)$, where α_{exp}, is the applied acceleration and d_1,d_2 are their respective diameters. This means that the residence time of large bubbles in the column when acceleration increases becomes significantly limited compared to that of small ones. Considering that the faster large bubbles carry a great percentage of the total desorbed gas volume, this explains why the resulting instantaneous local volumetric gas fraction decreases with acceleration. Regarding the effect of dissolution pressure, the present experimental findings show that desorbed gas fraction increases with pressure due to higher liquid supersaturation. In general, the gas volume fraction takes small values (<2.5%) implying that there is one-way coupling between liquid and gas flow fields. Hence, the residence time distributions measured in the absence of bubbles (Fig. 4) hold approximately also when bubbles are present.

The shape of curves in Fig. 6 suggests a power law equation $\varepsilon = b \cdot \alpha_{exp}^n$ for describing the decrease of volumetric gas fraction with acceleration, regardless of the dissolution pressure. The coefficient (b) and the exponent (n) of this equation vary with the applied dissolution pressure (P) ($b = -2 \cdot 10^{-5} \cdot P^2 + 0.0165 \cdot P - 1.314$ and $n = -5 \cdot 10^{-6} \cdot P^2 + 2 \cdot 10^{-3} P + 0.22$, at $z/D = 7.5$).

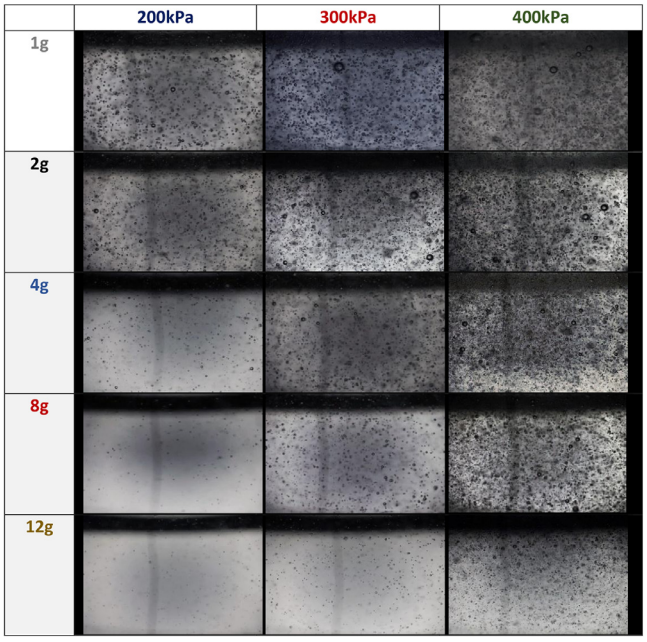

Fig. 7. Bubble images taken at the end of the injection period, at $z/D = 7.5$ and for all the examined accelerations and dissolution pressures.

Experimental data at $z/D = 2.5$ represent the bubbly flow at the mixing region of the column. Comparison of the corresponding values at $z/D = 7.5$ and $z/D = 2.5$ indicates a profile of desorbed gas along the column height for different experimental conditions. In the case of 200 kPa, there is an increasing gas concentration gradient from the bottom towards the top of the column. This gradient becomes steeper for higher acceleration values. Under hypergravity conditions, bubbles buoyancy velocity is important compared to the low liquid velocity at 200 kPa (Table 1). As a result, during injection degassing bubbles can escape from the liquid recirculation loop at the mixing region at the bottom part of the column. Under the pressure of 300 kPa, measurements at the two heights indicate that the desorbed gas phase is distributed quite uniformly along the column. The slight increase of gas fraction at $z/D = 7.5$ can be partially attributed to bubbles expansion due to the decrease of hydrostatic pressure as they move from the bottom to the top of the column. Unfortunately we had only measurements at $z/D = 7.5$ for the 400 kPa group. In this case, the buoyant bubbles velocity is not so important compared to the intense velocity of the liquid. Therefore, bubbles are expected to get trapped in the liquid recirculation loop and accumulate in the column mixing region.

3.3. Bubbles size distributions

Fig. 7 presents typical images of the bubbly liquid during degassing at $z/D = 7.5$ along the column, for all the examined accelerations and dissolution pressures. These images are captured at the end of the injection period, so they refer to the same injected liquid volume. From a quick glance, it is apparent that the number of bubbles decreases with the acceleration and increases with the dissolution pressure. These observations agree with the gas fraction measurements presented in the previous figures.

To investigate whether the increase of gas fraction during injection, Fig. 5, is associated with a change in bubbles size, bubble size distributions (BSD) are displayed at different time instants

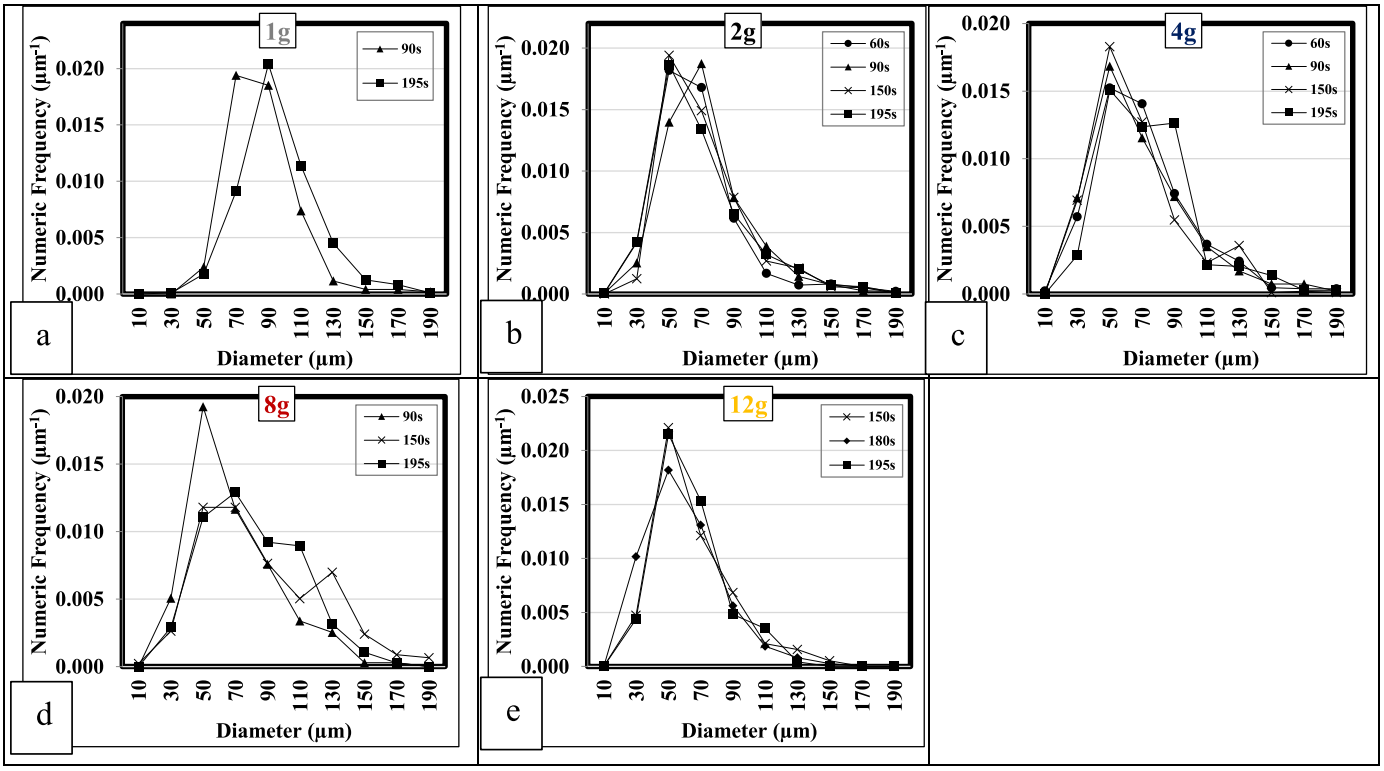

Fig. 8. Bubble size distributions at different time instants during the injection period under 300 kPa dissolution pressure and (a) 1 g, (b) 2 g, (c) 4 g, (d) 8 g and (e) 12 g applied accelerations.

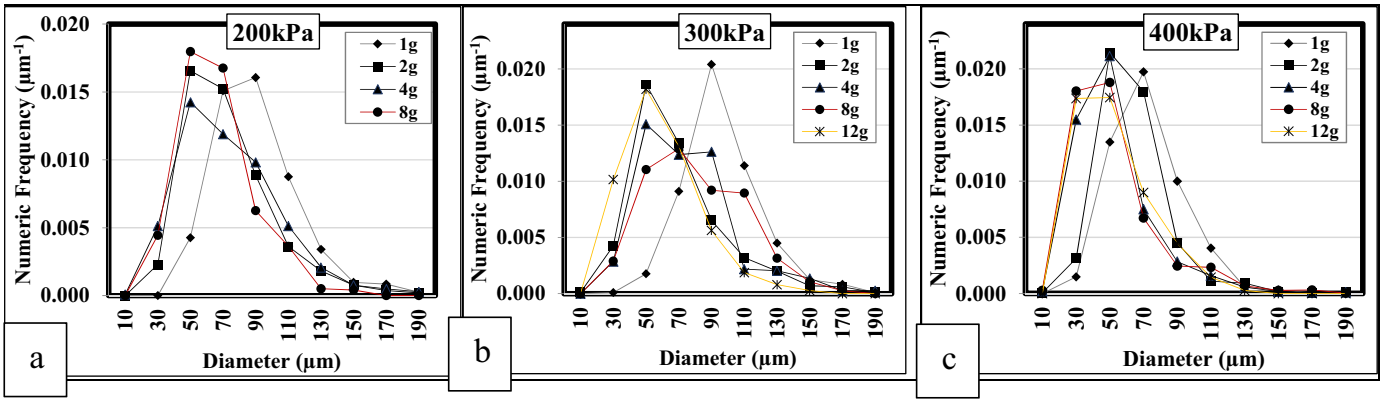

Fig. 9. Bubble size distributions under various accelerations and dissolution pressures (a) 200 kPa, (b) 300 kPa and (c) 400 kPa, at the end of the injection period.

along the injection period in Fig. 8. To avoid data overcrowding, Fig. 8 displays only results for the dissolution pressure of 300 kPa. The presented size distributions show that bubble size remains the same during the whole injection period for all the examined accelerations. This holds also for the cases of 200 kPa and 400 kPa (not shown). The observation that the size of degassing bubbles is not affected by the increasing concentration of desorbed gas during injection implies that once bubbles reach a certain size thereafter it is their number that increases and not their size. This means that bubbles do not coalesce inside the column (since turbulent coagulation is limited for low gas volume fractions, Lyklema, 2005) and that the growth of bubbles is exclusively attributed to desorption, i.e., mass transfer.

The effect of hypergravity acceleration on the size of degassing bubbles under different dissolution pressures is illustrated in Fig. 9. As acceleration increases, the distributions shift slightly towards smaller bubble sizes. This trend is more evident in the case of 400 kPa. Before questioning the effect of acceleration on the growth of degassing bubbles, one must quantify the effect of hydrostatic pressure on bubbles shrinkage/expansion. Since the hydrostatic pressure at the measuring location increases with the applied acceleration, the volume of a bubble is expected to change, too, according to the ideal gas law. Considering the working conditions of the present experiments, the diameter of a bubble at $z/D = 7.5$ under terrestrial gravity (d_{1g}) becomes 0.955 times smaller when exposed to 12 g (d_{12g}) based on the following calculations Eq. (2):

$$\frac{P_{1g}}{P_{12g}} = \left(\frac{d_{12g}}{d_{1g}}\right)^3 \rightarrow \frac{P_{atm} + P_{h,1g}}{P_{atm} + P_{h,12g}} = \left(\frac{d_{12g}}{d_{1g}}\right)^3 \rightarrow d_{12g} = 0.955 \cdot d_{1g} \tag{2}$$

where P_{1g} and P_{12g} are the pressures developed under 1 g and 12 g accelerations at the measuring location.

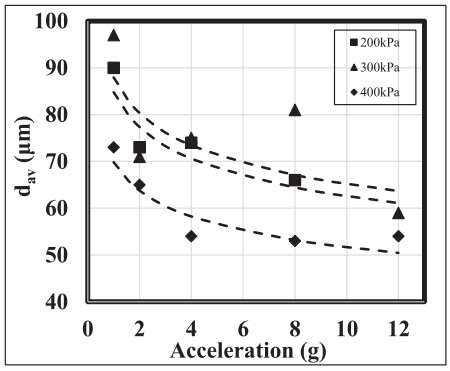

Fig. 10. Average size of degassing bubbles at the end of the injection period under various applied accelerations and dissolution pressures.

P_{atm} is the atmospheric pressure.
$P_{h,1g}$ and $P_{h,12g}$ are the liquid hydrostatic pressures developed under 1 g and 12 g accelerations at the measuring location.

However, the proportionality factors resulting from the experimental data are much lower, implying that the decrease of bubble size under high acceleration is dictated by other factors ($d_{av,12g}/d_{av,1g}$ is ~0.6 and ~0.73 for 300 kPa and 400 kPa, respectively, where $d_{av,12g}$ and $d_{av,1g}$ are the bubble average diameters for the corresponding accelerations). For the case of 200 kPa no BSD is computed under 12 g acceleration because the low bubble population density that does not allow statistically confident estimations. As already discussed, under high acceleration levels the residence time of bubbles in the column is short owing to the bubbles increased buoyant velocity. Hence, the smaller size of degassing bubbles may be attributed to the limited available time for mass transfer. Furthermore, deviations among the velocities of different sized bubbles accentuate under high accelerations and thus the residence time of large bubbles is much less than that of small bubbles. As a result, the insignificant numeric frequency of large bubbles shifts the distributions to smaller bubble diameters.

The correlation between the applied acceleration and the size of degassing bubbles is illustrated in Fig. 10. This figure presents the average bubble diameters under the examined accelerations and dissolution pressures. The dashed lines are smoothing lines passing through the data. These lines indicate a decreasing trend of bubbles size with acceleration for every dissolution pressure. However, the effect of dissolution pressure on bubble size is not so straightforward. According to literature, the size of bubbles generated during liquid degassing decreases with increasing dissolution pressure (Oikonomidou et al., 2018; De Rijk et al., 1994; Takahashi et al., 1979). This happens because upon decompression the concentration of excess dissolved gas in the liquid (supersaturation) increases proportionally with the dissolution pressure but at the same time the nucleation rate increases much more with supersaturation in a nonlinear fashion (Goldman, 2008). In the present work, even though the smallest degassing bubbles form indeed under the highest dissolution pressure (400 kPa), the transition from 200 kPa to 300 kPa does not comply with the aforementioned description. The fact that bubbles created under 200 kPa are just slightly smaller than those under 300 kPa may be attributed to the flow velocity. In the case of 200 kPa, the buoyant velocity of bubbles is significant compared to the low velocity of the liquid flow. Hence, at hypergravity conditions large bubbles escape easily from the streamlines of the liquid recirculation loop and move towards the free surface, leaving behind small bubbles. In the case of 400 kPa, Oikonomidou et al. (2018), measuring at a higher column ($z/D = 22.5$) and exclusively for 1 g conditions, have detected not only small bubbles (d_{av} ~60 μm) but also large bubbles (d_{av} ~350 μm). The presence of the latter has been attributed to coalescence phenomena dictated by gravitational acceleration in the plug flow region at the higher parts of their column. These phenomena are absent in the present shorter column.

3.4. Gas desorption efficiency

Fig. 11 shows the concentration of dissolved oxygen in the liquid stream exiting the degassing column during the whole injection period, for all the examined conditions. The first part of injection up to the marked vertical dashed line corresponds to the time needed for the injected stream to reach the measuring location (Dissolved Oxygen optical probe). After that part, the dissolved oxygen increases due to the continuous injection of supersaturated liquid to the column. The thermodynamic concentration of dissolved oxygen that corresponds to liquid full saturation at 25 °C and 101.35 kPa is 8.26 mg/L (Fogg and Gerrard, 1991). Apparently, all the curves lie above this value, meaning that both the preexisting liquid inside the Dissolved Oxygen (DO) vessel and the initial liquid inside the column (DO values right after the dashed line) are slightly supersaturated (~ 15%) already before injection. However, it must be stressed that this initial supersaturation is not adequate to trigger nucleation of degassing bubbles (Delale et al., 2003). Furthermore, the increasing trend of DO with time indicates that the residence time of the injected liquid in the column does not suffice for its complete degassing.

The final extent of liquid degassing can be calculated based on the DO measurements at the exit of the column at the end of the injection period (DO_{final}). Liquid Degassing Degree (%) equals

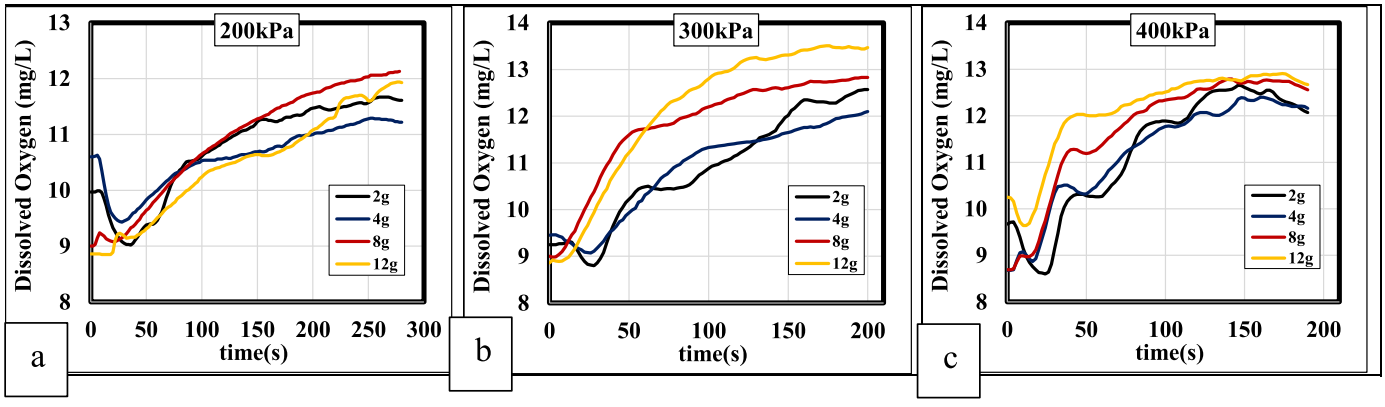

Fig. 11. Dissolved oxygen concentration in the liquid overflow stream during a complete run under various accelerations and dissolution pressures (a) 200 kPa, (b) 300 kPa and (c) 400 kPa.

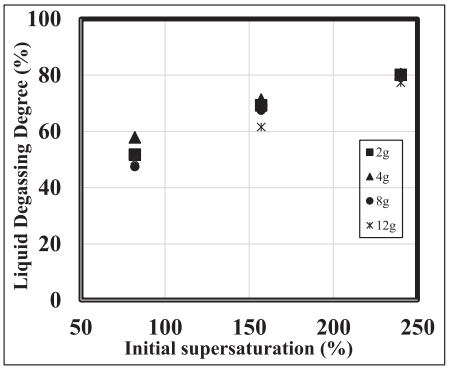

Fig. 12. The Liquid Degassing Degree under different accelerations and initial supersaturations.

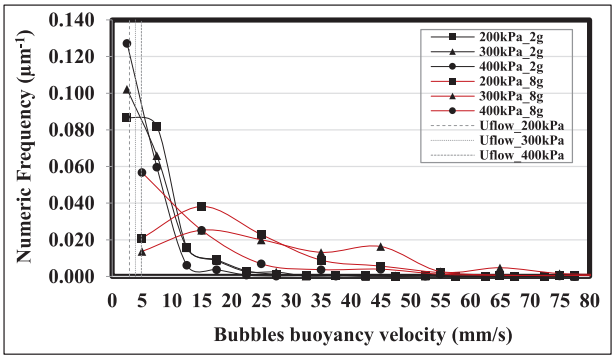

Fig. 13. Probability density functions of bubbles buoyancy velocity for all the applied dissolution pressures, under the accelerations of 2 g and 8 g.

$\frac{DO_{initial}-DO_{final}}{DO_{initial}-DO_{sat}} \cdot 100$, where $DO_{initial}$ is the concentration of dissolved oxygen in the compressed liquid volume in the saturator before injection to the degassing column and DO_{sat} is the thermodynamic concentration of dissolved oxygen corresponding to full saturation at 25 °C and 101.35 kPa. Initial supersaturation (%) equals $\frac{DO_{initial}-DO_{sat}}{DO_{sat}} \cdot 100$. Fig. 12 shows the Liquid Degassing Degree for different initial supersaturations, for all the examined hypergravity accelerations. Before injection, the compressed liquid in the saturator attains initial supersaturation of 82%, 157% and 240% for gas pressures 200 kPa, 300 kPa and 400 kPa, respectively. It is seen that the efficiency of liquid degassing increases significantly with the initial supersaturation. This is because supersaturation is the driving force of liquid degassing (Karapantsios et al., 2008), and when supersaturation increases mass transfer accelerates. Furthermore, Fig. 12 shows that the Liquid Degassing Degree does not vary so much with the applied acceleration. This means that the level of applied acceleration does not affect the mass transfer during the degassing of a flowing liquid.

4. Discussion

To describe the occurred phenomena in view of the experimental observations some preliminary discussion and calculations are needed. It is well known that degassing air bubbles have different composition than atmospheric air because oxygen desorbs differently than nitrogen and this should be accounted for in a detailed growth model. However, considering air as a single component is acceptable for the approximate calculations required here.

Bubble growth occurs mainly due to diffusion of dissolved gas in the liquid. The pure diffusion rate is enhanced by several types of convective contributions: i) convection created by bubble growth itself, ii) convection created by buoyant motion and iii) convection created by turbulent fluctuations of the fluid flow. The second and third types are important only when a bubble is relatively large so they are not discussed further. The first type of convection depends on the Foaming number (F_m) which is the ratio of excess concentration of dissolved gas over gas density (Divinis et al., 2004). This number takes values around 0.015, 0.03 and 0.045 for the three dissolution pressures of 200 kPa, 300 kPa and 400 kPa, respectively. These values are quite small so convection of type (i) can be ignored as well. The evolution of bubble radius (R_b) for diffusion dominated growth is given as $R_b = (2 \cdot F_m \cdot D_m \cdot t)^{0.5}$, where D_m is the diffusivity of gas in the liquid (Scriven, 1958). A rough calculation shows that bubbles with diameters of the order of 100 μm require a growth time between 10–30 s. This bubble growth time is smaller than the liquid residence time in the column. This indicates that in the present experiments, where most bubbles are even smaller than 100 μm, bubbles reach their final size too soon in the intense mixing region. So, the imposed hypergravity acceleration does not really influence bubble growth.

Another important variable that must be determined is the buoyancy velocity of bubbles. Since bubbles of the present size in a not-specially treated water can be considered to have an immobile interface, their buoyancy velocity can be computed by introducing a correction factor to the Stokes equation, accounting for their non-zero Reynolds number (Nguyen and Schulze, 2003). The resulting formula is presented in the Appendix. Some indicative probability density functions of buoyancy velocities are presented in Fig. 13, together with the flow velocities under the three working pressures. Fig. 13 shows that bubbles velocity decreases with the dissolution pressure and increases with the acceleration. Moreover, it indicates that bubbles velocity is more important compared to the flow velocity under lower dissolution pressures.

With the above information (experimental and calculated) at hand, the following possible physical picture arises:

Nucleation occurs only in the jet region where supersaturation is large. According to Maeda et al. (2015), cavitation in the constriction of the nozzle may also affect the number of nuclei, however this remains an unclear issue. In any case, the number of generated nuclei is a function of dissolution pressure.

The produced nuclei are transferred to the intense mixing region of the column where they grow fast with respect to their residence time in the flow. This fast growth is compatible with the constant, with respect to time, bubble size distributions observed experimentally (Fig. 8). The shape of the residence time distribution curves explains why there are no bubbles of small size at the measuring location ($z/D = 7.5$). The fact that there is no acceleration effect on the degassing efficiency (Liquid Degassing Degree) implies that bubble growth is independent from the acceleration magnitude. The smaller size of bubbles (Fig. 10) and the lower local volumetric gas fraction (Fig. 6) observed at higher accelerations, are not attributed to the restricted bubble/liquid contact time but to the strong correlation between bubble velocity and bubble size. Therefore, acceleration does not inhibit the process of mass transfer growth but it limits the instantaneous volumetric concentration of the generated gas phase within the flow by increasing the rate of bubbles departure to the free surface.

Regarding space applications, the above indicates that in the occasion of liquids that degas at hypergravity conditions (during the launch or re-orbiting of space vehicles), bubbles sliding along solid surfaces or bubbles dispersing in a liquid jet depend on their buoyant velocity. Regarding terrestrial applications, the number and size of degassing bubbles in industrial processes can be controlled by carefully imparting hypergravity accelerations, e.g., by centrifugation. It must be noted that the results of the present work cannot be straightforwardly applied to a liquid other than water. This

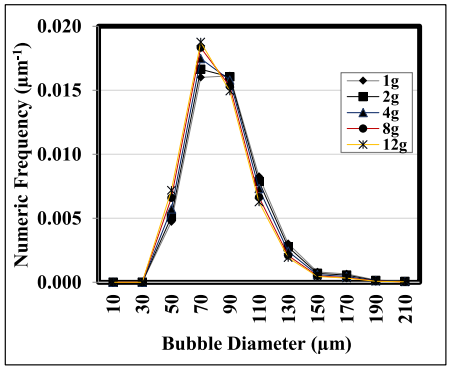

Fig. 14. Resulting bubble size distributions under different accelerations, as indicated by the proposed qualitative model.

is because the physicochemical properties of the liquid affect all the involved sub-processes (nucleation, growth, coalescence, buoyant motion) in a complicated way.

The findings of this study allow the construction of a very simple qualitative model for the effect of acceleration on bubble growth. Let us consider the intensively mixed region of the column. Bubble growth is said to occur at smaller time scales than its residence time in the column so at this level of approximation there should be a bubble size distribution $f_0(d)$ at 1 g conditions that depends only on the dissolution pressure and can be considered as an inlet parameter for this region. Such a simple approach is compatible with the observed increase of gas fraction and the constant size distributions during the injection period. A simple solution for the outlet bubble size distribution at different accelerations is:

$$f_{a_{exp}}(d) = f_0(d) \Big/ \left(1 + \lambda \cdot \frac{U_b(d)}{U_{flow}}\right) \tag{3}$$

where d: is the bubble diameter.

$f\alpha_{exp}(d)$: is the resulting bubble size distribution under some experimental acceleration (α_{exp}).

λ: is a parameter between 0 and 1 that depends on the exact type of flow in the considered region (in this case $\lambda = 0.1$).

The effect of acceleration on bubble size emerging from Eq. (3) is illustrated in Fig. 14. It is apparent that Eq. (3) predicts the shift of the distributions to smaller diameters and the reduction of gas volume fractions with the acceleration, as it has been observed experimentally. Moreover, Eq. (3) unravels (at least qualitatively) the effect of different parameters on bubble size distributions. The supersaturation acts on $f_0(d)$, the liquid flow rate on U_{flow} and the acceleration on $U_b(d)$.

5. Conclusions

The present work investigates the formation of gas phase due to degassing of a pressurized flowing liquid in hypergravity conditions. The pressurized liquid becomes supersaturated with dissolved gas as it decompresses into an open column, filled with stagnant unsaturated liquid. Before injection, the liquid is partially saturated with dissolved gas under 200 kPa, 300 kPa and 400 kPa. Hypergravity accelerations of 2 g, 4 g, 8 g and 12 g are applied artificially, using the Large Diameter Centrifuge (LDC) facility of ESA/ESTEC. A custom device is constructed in compliance with safety regulations and spatial restrictions of the LDC, for the execution of liquid degassing experiments. Increasing the magnitude of hypergravity acceleration results in the formation of slightly smaller bubbles and the desorption of lower volumetric gas fractions during liquid degassing. The above observations are attributed to the increased bubbles buoyancy velocity and not to mass transfer restrictions, since the total extent of degassing is not affected by acceleration. Regarding the effect of dissolution pressure on liquid degassing, the concentration of desorbed gas increases with pressure and the generated two-phase flow gets homogeneously distributed along the column. Experimental findings show that hypergravity accelerations in space applications (during the launch or re-orbiting of space vehicles) may favor heat removal in cooling systems, since then degassing bubbles travel faster and do not accumulate in the flow loop of micro-channels. From a terrestrial perspective, centrifugal systems can be adopted in industrial applications where the concentration of degassing bubbles should be minimized.

Acknowledgments

This study is funded by the European Space Agency (NPI Project: Bubble dynamics during degassing of liquids - contract no.: 4000108790/13/NL/PA) and carried out under the umbrella of COST Action MP1106: 'Smart and green interfaces- from single bubbles and drops to industrial, environmental and biomedical applications' and COST Action MP1305: 'Flowing matter'. We would like to thank Dr. Kostantinos Zacharias for his technical and scientific support regarding the electrical impedance spectroscopy measurements and Mr. Triantafillos Tsilipiras for his contribution in building the experimental setup. We would also like to thank Mr. Alan Dowson from ES-ESTEC-TEC-MMG for his technical support with LDC during this study. The view expressed herein can in no way be taken to reflect the official opinion of the European Space Agency.

Appendix. Formula for computation of bubble buoyancy velocity

The formula used to calculate the buoyancy velocity (U_b) for the present size of bubbles, results from the bubbles terminal velocity predicted by Stokes' law (U_{stokes}), corrected by Archimides number (Ar) with respect to the not-specially treated water and the non-zero bubbles Reynolds number (Nguyen and Schulze, 2003). The bubbles buoyancy velocity formula is presented below:

$$U_b = \frac{U_{stokes}}{1 + \frac{\frac{Ar}{96}}{\left(1+0.079 \cdot Ar^{0.749}\right)^{0.755}}}$$

where, $U_{stokes} = \frac{2 \cdot {R_b}^2 \cdot a_{exp} \cdot \rho_l}{9 \cdot \mu_l}$ is the bubbles terminal velocity predicted by Stokes' law.

$Ar = \frac{8 \cdot {R_b}^3 \cdot \rho_l^2 \cdot a_{\exp}}{\mu_l^2}$ is the Archimides number.

ρ_l is the density of water.

μ_l is the viscosity of water.

a_{exp} is the experimental acceleration.

R_b is the bubble radius.

References

Alshahrani, S.M., Morott, J.T., Alshetaili, A.S., Tiwari, R.V., Majumdar, S., Repka, M.A., 2015. Influence of degassing on hot-melt extrusion process. Eur. J. Pharm. Sci. 80, 43–52.

Beysens, D.A., van Loon, J.J.W.A., 2015. Generation and Applications of Extra-Terrestrial Environments on Earth. Rivers Publishers, Denmark.

Birdi, K.S., Kleinitz, W., 1998. Problems associated with dissolved atmospheric oxygen in crude oil at production facilities. Oil Gas Eur. Mag. 24 (2), 25–28.

Burns, S.E., Yiacoumi, S., Tsouris, C., 1997. Microbubble generation for environmental and industrial separations. Sep. Purif. Technol. 11 (3), 221–232.

Caputo, G., Adami, R., Reverchon, E., 2010. Analysis of dissolved-gas atomization: supercritical CO2 dissolved in water. Ind. Eng. Chem. Res. 49 (19), 9454–9461.

Chen, C., 1993. Cope with dissolved gases in pump calculations. Chem. Eng. 100 (10), 106–112.
Chen, Y.M., Wu, S.C., Chu, C.I., 2001. Thermal performance of sintered miniature heat pipes. Heat Mass Transf. 37 (6), 611–616.
Delale, C.F., Hruby, J., Marsik, F., 2003. Homogeneous bubble nucleation in liquids: the classical theory revisited. J. Chem. Phys. 118 (2), 792–806.
Divinis, N., Karapantsios, T.D., Kostoglou, M., Panoutsos, C.S., Bontzoglou, V., Michels, A.C., Sneep, M.C., Bruijn, R., Lotz, H., 2004. Bubbles growing in supersaturated solutions at reduced gravity. AIChE J. 50 (10), 2369–2382.
Edzwald, J.K., 2007. Developments of high rate dissolved air flotation for drinking water treatment. J. Water Supply Res. Technol. 56 (6–7), 399.
Evgenidis, S., Karapantsios, T.D., 2015. Effect of bubble size on void fraction fluctuations in dispersed bubble flows. Int. J. Multiph. Flow 75, 163–173.
Fogg, P.G.T., Gerrard, W., 1991. Solubility of Gases in Liquids. John Wiley & Sons, New York.
Goldman, S., 2008. The stability of bubbles formed from supersaturated solutions, and homogeneous nucleation of gas bubbles from solution, both revisited. J Phys Chem B. 112 (51), 16701–16709.
Hearn, H.C., Coyle, D., 2007. Influence of dissolved gas on on-orbit thruster performance fluctuations. In: Joint Propulsion Conference, 6, pp. 5582–5591.
Hosokawa, S., Tanaka, K., Tomiyama, A., Maeda, Y., Yamaguchi, S., Ito, Y., 2009. Measurement of micro bubbles generated by a pressurized dissolution method. J. Phys. 147, 1–10.
Huang, Z., Yiming, S., Shiga, S., Nakamura, H., Karasawa, T., Nagasaka, T., 1994. Atomization behavior of fuel containing dissolved gas. Atom. Sprays 4 (3), 253–262.
Karapantsios, T.D., Kostoglou, M., Divinis, N., Bontozoglou, V., 2008. Nucleation, growth and detachment of neighboring bubbles over miniature heaters. Chem. Eng. Sci. 63 (13), 3438–3448.
Karapantsios, T.D., Evgenidis, S.P., Zacharias, K., Mesimeris, T., 2016. Method for the detection and characterization of bubbles in liquids and device therefor, resp. system. European Patent Office, 3005942 A1.
Kulkarni, A.A., Joshi, J.B., 2005. Bubble formation and bubble rise velocity in gas-liquid systems: a Review. Ind. Eng. Chem. Res. 44, 5873–5931.
van Loon, J.J.W.A., Folgering, E.H., Bouten, C.V., Veldhuijzen, J.P., Smit, T.H., 2003. Inertial shear forces and the use of centrifuges in gravity research. What is the proper control? J. Biomech. Eng. 125 (3), 342–346.
van Loon, J.J.W.A., Krausse, J., Cunha, H., Goncalves, J., Almeida, H., Schiller, P., 2008. The large diameter centrifuge, LDC, for life and physical sciences and technology. Life Space Life Earth 553.
Liger-Belaira, G., Sternenberg, F., Brunner, S., Robillard, B., Cilindre, C., 2015. Bubble dynamics in various commercial sparkling bottled waters. J. Food Eng. 163, 60–70.
Lioumbas, J.S., Karapantsios, T.D., 2014. Effect of increased gravitational acceleration in potato deep-fat frying. Food Res. Int. 55, 110–118.
Lopes, P., Silva, M.A., Pons, A., Tominaga, T., Lavigne, V., Saucier, C., Darriet, P., Teissedre, P.L., Dubourdieu, D., 2009. Impact of oxygen dissolved at bottling and transmitted through closures on the composition and sensory properties of a sauvignon blanc wine during bottle storage. J. Agric. Food Chem. 57 (21), 10261–10270.
Lyklema, J., 2005. Fundamentals of interface and colloid science. soft Colloids 5 New York.
Maeda, Y., Hosokawa, S., Baba, Y., Tomiyama, A., Ito, Y., 2015. Generation mechanism of micro-bubbles in a pressurized dissolution method. Exp. Therm. Fluid Sci. 60, 201–207.
Mori, B.K., 1998. Studies of Bubble Growth and Departure from Artificial Nucleation Sites Ph.D. Thesis, Department of Mechanical and Industrial Engineering. University of Toronto.
Nauman, E.B., Buffham, B.A., 1983. Mixing in Continuous Flow System. Wiley, New York.
Nguyen, A.V., Schulze, H.J., 2003. Colloidal Science of Flotation. CRC Press, United States.
Oikonomidou, O., Evgenidis, S.P., Kostoglou, M., Karapantsios, T.D., 2018. Degassing of a pressurized liquid saturated with dissolved gas when injected to a low pressure liquid pool. Exp. Therm. Fluid Sci. 96, 347–357.
Papadopoulou, V., Eckersley, R.J., Balestra, C., Karapantsios, T.D., Tang, M-X., 2013. A critical review of physiological bubble formation in hyperbaric decompression. Adv. Colloid Interface Sci. 191-192, 191–192.
Ponasse, M., Dupre, V., Aurelle, Y., Secq, A., 1998. Bubble formation by water release in nozzle II: influence of various parameters on bubble size. Water Res. 32 (8), 2498–2506.
De Rijk, S.E., den Blanken, J.G., 1994. Bubble size in flotation thickening. Water Res. 28 (2), 465–473.
Radzuan, M.R.A., Belope, A-B., Thrope, R.B., 2016. Removal of fine oil droplets from oil-in-water mixtures by dissolved air flotation. Chem. Eng. Res. Des. 115, 19–33.
De Sain, J.D., Brady, B.B., Curtiss, T.J., Greenberg, L.T., Smith, M.B., Villahermosa, R.M., 2015. Solubility of pressurant gases in liquid hydrazine at elevated. J. Propul. Power 31 (4), 1193–1203.
Sathyan, K., Hsu, H.Y., Lee, S.H., Gopinath, K., 2010. Long-term lubrication of momentum wheels used in spacecrafts—an overview. Tribol. Int. 43 (1–2), 259.
Scriven, L.E., 1958. On the dynamics of phase growth. Chem. Eng. Sci. 10 (1), 1–13.
Shannon, W.T., Buisson, D.H., 1980. Dissolved air flotation in hot water. Water Res. 14 (7), 759–765.
Soto, A.M., Prosperetti, A., Lohse, D., van der Meer, D., 2017. Gas depletion through single gas bubble diffusive growth and its effect on subsequent bubbles. J. Fluid Mech. 831, 474–490.
Straub, J., 2005. Bubble - bubbles – boiling. Microgravity Sci. Technol. 16, 242–248.
Sunol, F., Gonzalez-Cinca, R., 2015. Effects of gravity level on bubble formation and rise in low-viscosity liquids. Phys. Rev. E 91, 053009.
Takahashi, T., Miyahara, T., Mochizuki, H., 1979. Fundamental study of bubble formation. J. Chem. Eng. Jpn. 12 (4), 275–280.
Talaia, M.A.R., 2007. Terminal velocity of a bubble rise in a liquid column. Int. J. Phys. Math. Sci. 1 (4), 220–224.
Vlyssides, A.G., Mai, S.T., Barampouti, E.P., 2004. Bubble size distribution formed by depressurizing air-saturated water. Ind. Eng. Chem. Res. 43 (11), 2775–2780.
Zabulis, X., Papara, M, Chatziargyriou, A., Karapantsios, T.D., 2007. Detection of densely dispersed spherical bubbles in digital images based on a template matching technique: application to wet foams. Colloids Surf. A 309 (1–3), 96–106.